J. Fluid Mech. (1984), *vol.* 147, *pp.* 333–352
Printed in Great Britain

Self-excited jet: upstream modulation and multiple frequencies

By MICHAEL LUCAS AND DONALD ROCKWELL
Department of Mechanical Engineering and Mechanics, Lehigh University, Bethlehem, Pennsylvania 18015

(Received 26 October 1983 and in revised form 24 May 1984)

The self-excited oscillation of a planar jet impinging upon a wedge can give rise to not simply a single, but as many as seven well-defined frequency components in the range of Reynolds-number (based on nozzle width and mean velocity) $250 \leqslant Re \leqslant 1150$. All of these components are traceable to the nonlinear distortion/interaction (i.e. sum and difference) frequencies of two primary components: the most stable frequency of the jet shear layer (β); and a low-frequency modulating component ($\frac{1}{3}\beta$).

The modulating component $\frac{1}{3}\beta$ arises from vortex–vortex interaction at the impingement edge. This interaction involves vortices of both like and opposite sense; the vortices of opposite sense to those of the incident shear layer arise from eruption of the viscous layer at the edge and tend to form counter-rotating vortex pairs with the incident vortices. The details of the vortex–vortex interaction pattern vary with Reynolds number; however, the pattern adjusts itself to maintain the modulating component $\frac{1}{3}\beta$. Its upstream influence strongly modulates the sensitive region of the shear layer at the jet nozzle lip. Consequently, the linear-growth region of the disturbance near the lip is dominated by the component $\frac{1}{3}\beta$, which eventually gives way to the most unstable component β further downstream.

1. Introduction

It is well known that impingement of a planar jet upon an edge can give rise to strongly coherent, self-sustained oscillations (see figure 1). Recent investigations of this class of flows, including related cases of mixing-layer and wake–edge interactions, are reviewed by Rockwell (1983). The framework established by Powell (1961), in which he defines the central features of these oscillations, continues to provide the basis for further studies. Figure 1 represents the fundamental characteristics of a typical self-sustaining oscillation: amplification of unstable disturbances in the shear layer of the jet associated with a downstream-travelling instability wave; impingement of the amplified disturbance (i.e. vorticity) field upon the wedge; upstream influence or 'feedback' of this unsteady interaction at the impingement edge; and conversion of this upstream influence to vorticity fluctuations in the sensitive region of the shear layer near the nozzle exit. These vorticity fluctuations are, in turn, amplified, and so on.

As discussed in detail by Powell (1961), and more recently by Rockwell (1983), these jet-edge flows exhibit jumps in oscillation frequency, as well as hysteresis, when the impingement lengthscale or velocity U is varied. Figure 1 represents these upward and downward jumps in frequency and the associated hysteresis loop for the case where flow velocity is first increased, then decreased, as indicated by the arrows.

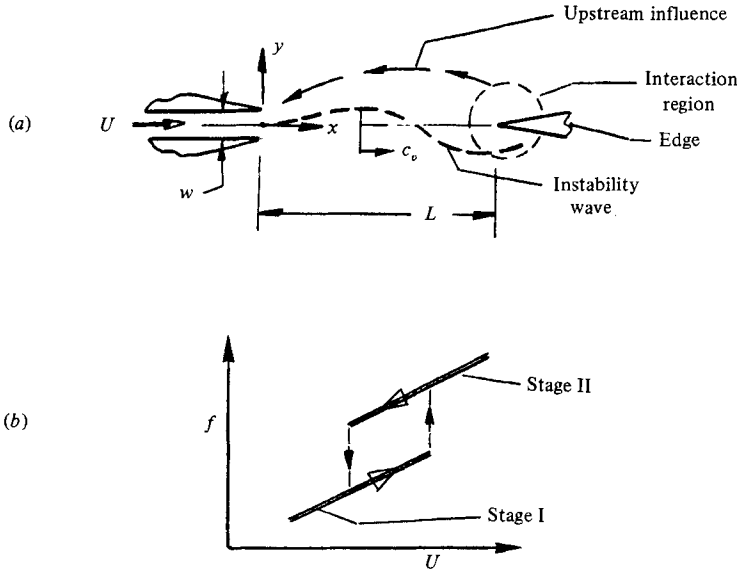

FIGURE 1. Schematics of (*a*) essential features of jet–edge oscillation; (*b*) frequency jumps, hysteresis and definition of stages I and II.

An inherent assumption in nearly all theoretical and experimental investigations carried out to date is that the oscillating jet possesses a single predominant frequency of oscillation. A notable exception is the study of Stegen & Karamcheti (1970), who showed that two frequency components may be present simultaneously; the additional component arises from the fact that the stage I component can persist into stage II (figure 1). Although one might detect only a single predominant frequency in the region well away from the edge where pressure measurements are typically made (see e.g. Powell 1961), a nonlinear oscillating jet should show existence of multiple frequencies and their interaction. The corresponding energy exchange between frequency components would influence the amplitude of the 'predominant' component of the jet, the distribution of the pressure field on the wedge, and the surrounding sound field as well.

In essence, the following crucial aspects remain uninvestigated: the spectral evolution of the jet from separation to impingement, including the possible interaction of primary frequency components yielding a number of additional components; detailed mechanics of vortex interaction at the edge, including distortion and severing of the incident jet vortices; possible interaction between an unstable vortex(ices) within the jet shear layer and a vortex(ices) arising from viscous effects at the wedge; and the consequence of the upstream influence that modulates the sensitive region of the shear layer near separation. In this investigation, we attempt to clarify these issues.

2. Experimental system

Experiments were carried out in a recirculating water tunnel whose test section housed the planar jet-nozzle–wedge system depicted schematically in figure 1. In order to ensure a fully developed flow at the nozzle exit for the range of Reynolds number under consideration ($250 \leqslant Re \leqslant 900$), the length of the parallel section of

the nozzle to its width was 68. To maximize two-dimensionality of the planar jet, the breadth-to-width ratio of the nozzle was 48. Further more, to minimize the influence of the upper and lower bounding walls of the test section, the ratio of the test-section height to nozzle width was 72. All experiments were conducted at an impingement length L to nozzle-width w ratio $L/w = 7.5$.

Considerable effort was expended to eradicate various contaminating effects of the flow system, including pulsations from the upstream and downstream plenum tanks of the water channel, and a free-surface resonance in the main test section. The result was an extremely low-disturbance-level system, verified by spectral analysis of hot-film measurements at the jet-nozzle exit; the fluctuation level lay below the noise threshold of the anemometry system of $\tilde{u}/U \sim 10^{-4}$. Here $\tilde{u}$ and $\tilde{v}$ denote root-mean-square values of the longitudinal and cross-stream velocity fluctuations.

With the exception of preliminary experiments, all velocity measurements were made with an LDA system having a 2 W argon-ion laser (backscatter mode) with a beam-expander module to maximize signal-to-noise ratio. Silicon carbide particles provided effective seeding, allowing use of the analog output of the frequency counter, and subsequent processing of the signal on an MINC minicomputer (LSI 11-03) with direct memory access. In performing spectral analyses of the fluctuating velocity signal, about 75 oscillation cycles were considered; moreover, the final spectral amplitudes were obtained by averaging eight of these spectra.

In obtaining flow visualization, food colouring was injected into the plenum region upstream of the jet nozzle, and the visualized field recorded using an Instar television system. Polaroid photos were then taken of the desired scenes, in order to show the essential features of an oscillation cycle.

3. Overview of flow mechanisms and dominant frequency components

Figure 2(*a*) provides an overview of the primary mechanisms and frequency components addressed here. For stage I oscillations, which occur at low values of Reynolds number, the jet oscillates with a single predominant frequency; we designate this component $\frac{1}{3}\beta$. At the edge, counter-rotating vortex pairs are formed at this same frequency $\frac{1}{3}\beta$, leading to an upstream disturbance that modulates the sensitive region of the shear layer near the nozzle exit at frequency $\frac{1}{3}\beta$.

In contrast to this clear predominance of the single frequency $\frac{1}{3}\beta$ in the growth of the shear layer and in the fedback signal occurring in stage I, stage II (figure 2*b*) involves two primary frequency components: β and $\frac{1}{3}\beta$. The streamwise growth of the jet shows vortex formation in the jet shear layer at its most unstable frequency β; however, this inherent instability of the jet is strongly modulated at the lower-frequency component $\frac{1}{3}\beta$ of stage I. The source of this low-frequency upstream influence is the interaction between successive vortices of characteristic frequency β in the vicinity of the leading edge of the wedge. They nest together at this location, the effective frequency is lowered, and predominant fedback disturbance is at frequency $\frac{1}{3}\beta$; of course there is also an upstream influence at frequency β as well. These frequency components represent only the most dominant ones; their interaction can give rise to as many as seven well-defined components.

Figure 2(*c*) shows the location of the predominant frequency components on the amplification factor $-\alpha_i$ versus frequency $\Omega = 2\pi f(\frac{1}{2}w/U)$ diagram; it represents the degree of amplification of $\tilde{v} \propto e^{-\alpha_i x}$. The frequency component β is close to the most amplified disturbance predicted on the basis of linear stability theory, while the frequency component $\frac{1}{3}\beta$ undergoes substantial amplification as well.

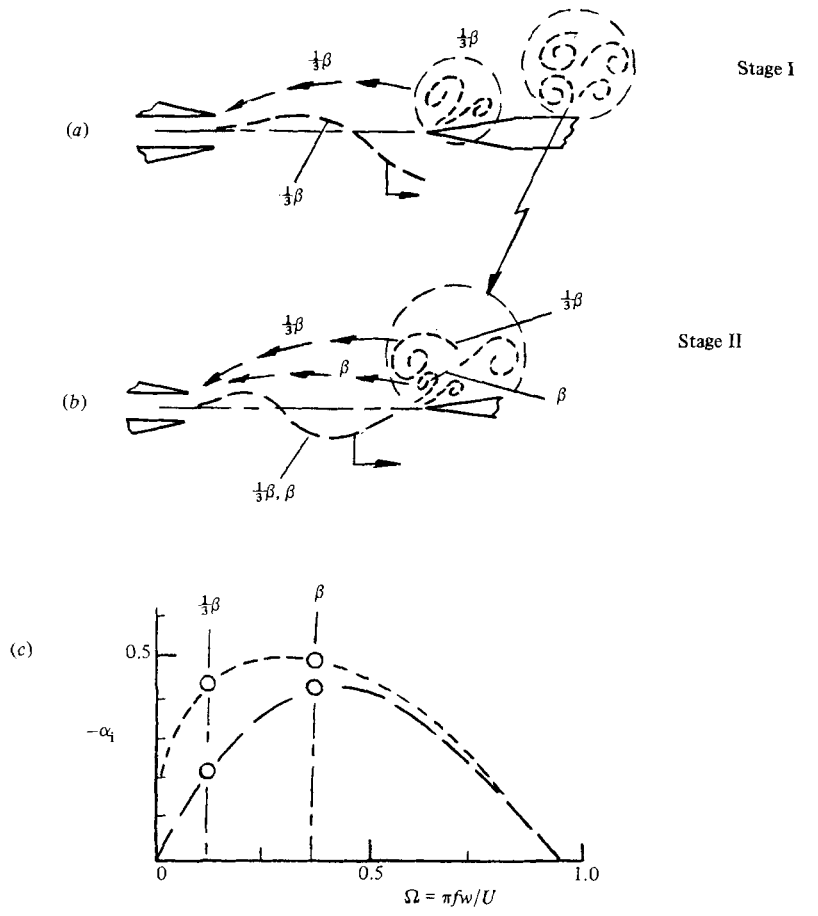

FIGURE 2. Illustration of (*a*) predominant frequencies of downstream-travelling instability wave, vortex formation/interaction at impingement edge, and upstream influence for stage I; (*b*) for stage II; (*c*) amplification factor for predominant frequencies of oscillation based on inviscid spatial (– – –) and transformed temporal (— — —) theories.

All these aspects will be addressed in the following, starting with visualization of the oscillating jet and instantaneous traces of fluctuating velocity within the jet. Then these mechanisms will be related to the time-averaged disturbance growth rates of the primary frequency components.

Visualization

Figures 3 (*a*, *b*, *c*) show vortex interaction patterns for one complete cycle of oscillation at $Re = 250$, 600 and 900 respectively. Dye was injected at the nozzle entrance in order to produce markers emanating from the upper and lower edges of the nozzle exit, thereby allowing visualization of the vortex evolution in the upper and lower regions of the shear layer. The six photos at each Re represent $\frac{5}{6}$ of a complete oscillation cycle, corresponding to times $t/T = 0, \frac{1}{6}, \frac{2}{6}, \ldots, \frac{5}{6}$, where T is the complete period of oscillation. We emphasize that the period T is determined by the total time for the modulated instability event to occur. For example, in stage I, where frequency $\frac{1}{3}\beta$ is dominant, the complete period T does not correspond to $1/\frac{1}{3}\beta$ because of

low-frequency modulation of the primary-vortex formation at $\frac{1}{3}\beta$. In the following, we discuss visualization details of these modulated instabilities.

The series of figure 3(*a*), representing 'stage I' oscillations, shows that each vortex originating from instability of the jet shear layer (i.e. A-type vortex) induces eruption of the viscous layer and formation of a vortex of opposite sense (i.e. B-type vortex). Frequency $\frac{1}{3}\beta$ corresponds to the rate at which the A-type vortices are formed at the leading edge; in other words the period $T_{\frac{1}{3}\beta}$ is the time interval between vortices A (at $t/T = 0$) and A″ (at $t/T = \frac{3}{6}$). Furthermore, the visualized 'stem' of the jet near the nozzle exit oscillates at frequency $\frac{1}{3}\beta$. (These observations agree with the predominance of the $\frac{1}{3}\beta$ component in the velocity–time traces of figure 5.) However, the period of the complete oscillation cycle is twice the period $T_{\frac{1}{3}\beta}$ due to a subharmonic instability occurring further down the wedge. As shown in the fourth photo at $t/T = \frac{3}{6}$, there is an eventual merging together of the A and A″ vortices. The tendency towards this nesting of vortices is evident earlier in the cycle: at $t/T = \frac{1}{6}$, the vortex pair A–B tends to shoot away from the wedge; and at $t/T = \frac{2}{6}$ the vortex pair A″–B″ tends to move along the wedge.

Figure 4 shows an overview of this merging process. Consider the vortex pairs on the lower side of the wedge. In figure 4(*a*) the upstream pair is about to rest within the downstream one. Figure 4(*b*) reveals that the upstream counter-rotating pair passes beneath the downstream vortex that originally arose from free-shear-layer instability. Further scenes show completion of this process; it produces very large-scale vortices, as depicted in figure 4(*c*) (not part of this same sequence). The two vortices originally stemming from the unstable free shear layer have coalesced and allowed the vortex erupting from the boundary layer to pass beneath them. Extensive spectra of LDA measurements in the near region of the jet (small values of x/L) showed no evidence of this subharmonic component at $\frac{1}{6}\beta$ having a period $T_{\frac{1}{6}\beta}$. Since this subharmonic merging occurs well downstream of the leading edge, its role in the upstream influence is apparently overshadowed by the interaction of A-type vortices (figure 3; $Re = 250$) with the leading edge. The important point concerning this merging of vortices downstream of the edge, referred to as A–B and A″–B″ in figure 3 ($Re = 250$), is that it moves upstream towards the leading edge with increasing Re, where it exerts a pronounced influence upon the upstream jet dynamics.

In figure 3(*b*), representing 'stage II' oscillations at $Re = 600$, the series of photos shows that the vortices of the incident shear layer are more mature in the region upstream of the edge. Both A-type and B-type vortices now originate from instability of the free shear layer to form counter-rotating vortex pairs A′–B′ ($t/T = 0, \frac{1}{6}$) and A‴–B‴ ($t/T = \frac{4}{6}$) downstream of the leading edge. These pairs A′–B′ and A‴–B‴ merge with, then sweep beneath, the large-scale vortices A and A″ respectively. The complete period of the oscillation cycle is $\frac{1}{3}\beta$, corresponding to the rate of formation of large-scale vortices $A, A^{\mathrm{iv}}, \ldots$. The upstream influence of these large vortices at frequency $\frac{1}{3}\beta$ dominates the region of the jet near separation. From the photos of figure 3(*b*), it is also evident that each of the incident shear-layer vortices interacts with the edge, so we can expect substantial upstream influence at frequency β as well. This is confirmed by LDA measurements (discussed subsequently), and also by the time traces of figure 5 ($Re = 600$; $x/L = 0.05, 0.16$).

Figure 3(*c*), representing a higher-Reynolds-number ($Re \equiv 900$) oscillation, shows a somewhat different pattern of vortex interaction. Whereas the major share of vortex B‴ passes above the edge in figure 3(*b*), the corresponding vortex in figure 3(*c*) passes below the edge, and is designated as an A-type vortex, i.e. A‴. Its counterpart B‴ in figure 3(*b*) eventually merges with other vortices; in contrast, vortex A‴ in figure 3(*c*) does not. In fact, there appears to be a return to the B-type vortex

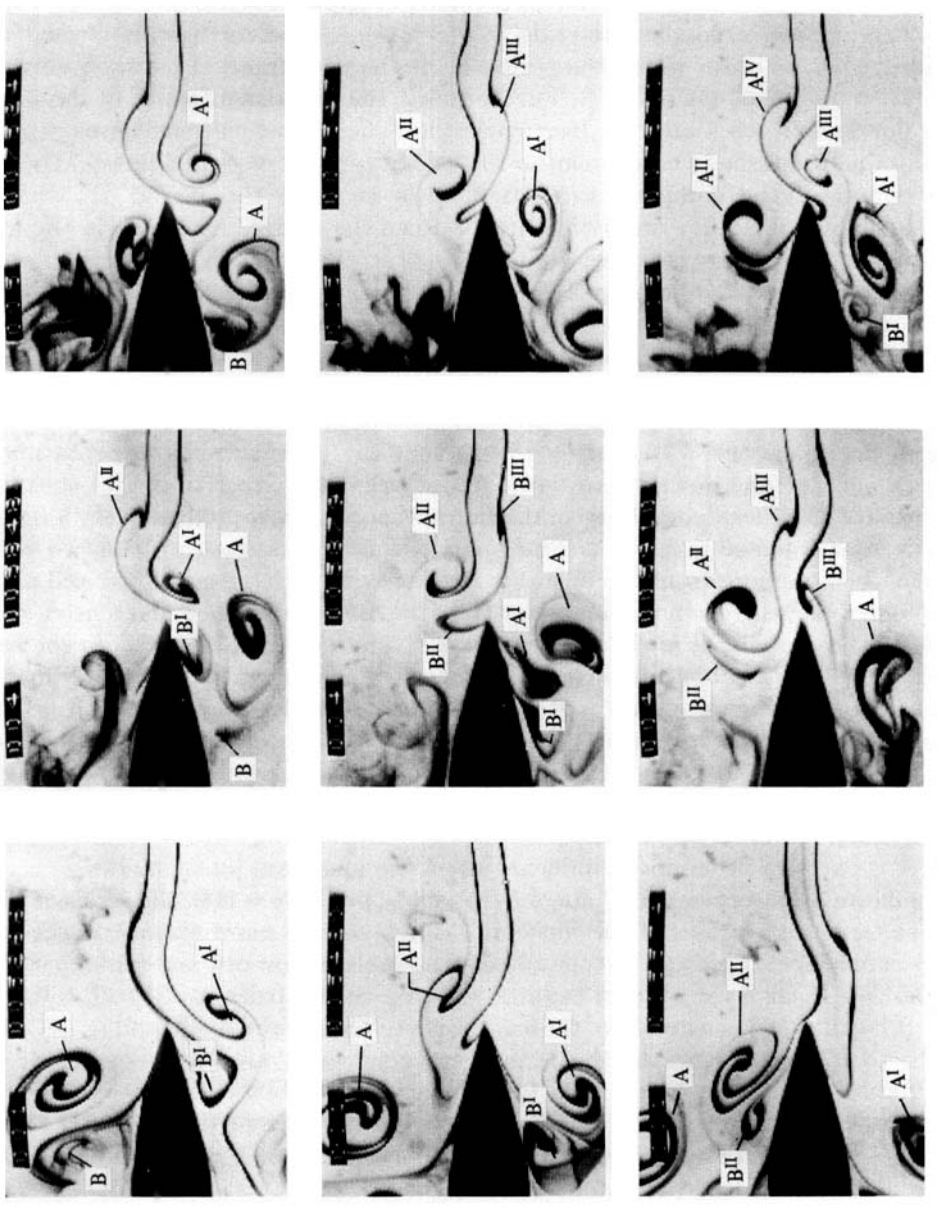
Re = 250
600
900
t/T = 0
1/8
2/8
A
B
A^I
B^I
A^II
B^II
A^III
B^III
A^IV

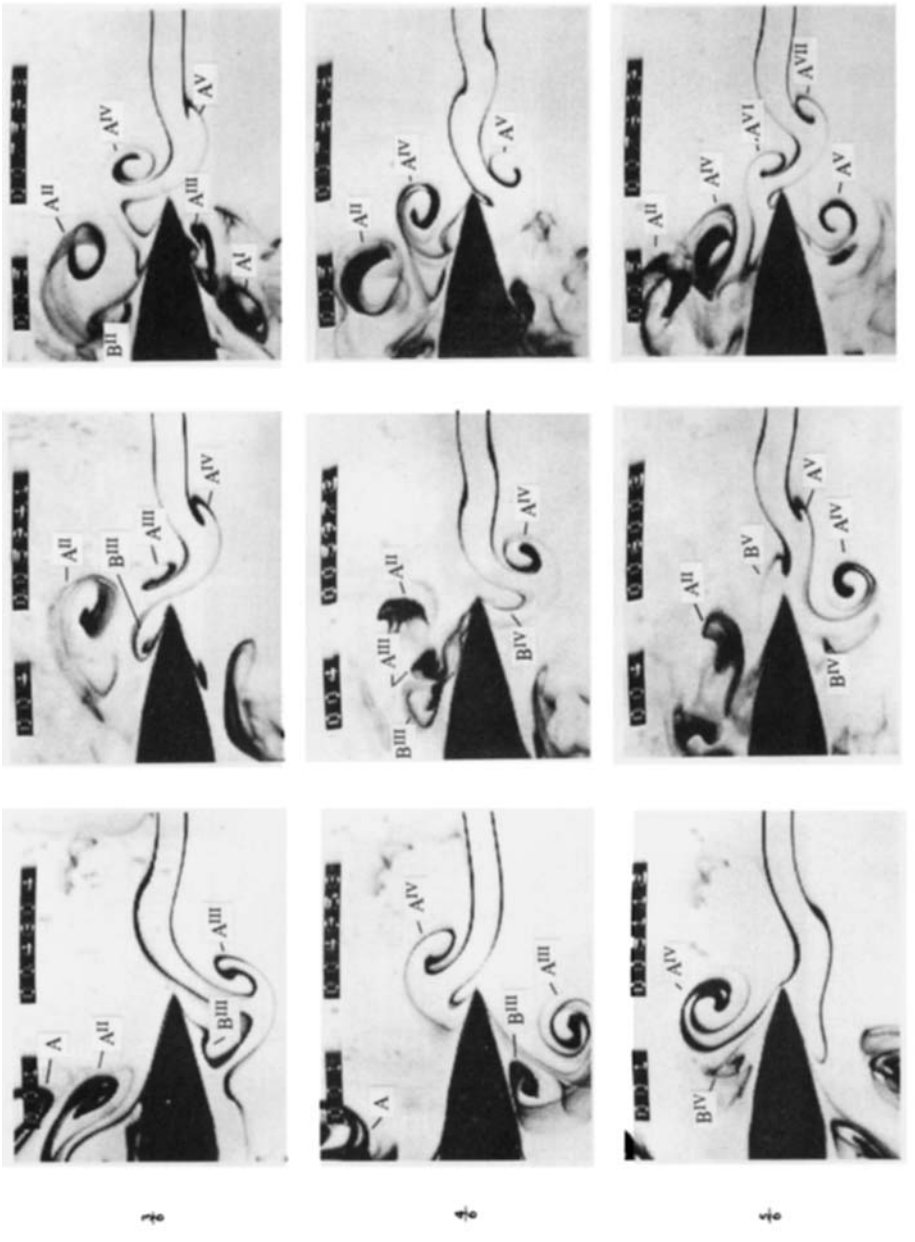

FIGURE 3. Visualization of one complete cycle of oscillation for (*a*) $Re = 250$ (stage I); (*b*) 600 (stage II); (*c*) 900.

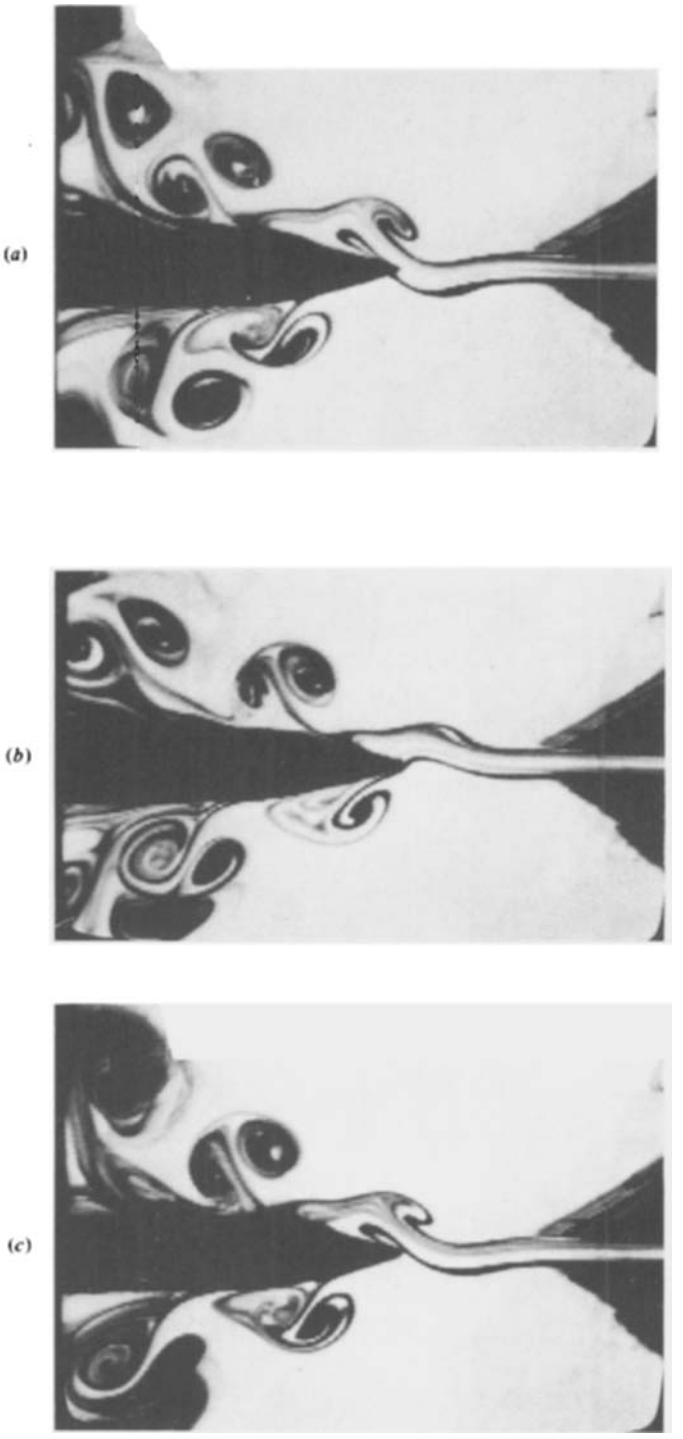

FIGURE 4. Secondary instability of counter-rotating vortex pairs at successive instants of increasing time (top to bottom); $Re = 300$.

generation shown in figure 3(*a*) (note vortices B, B′, and B″ in figure 3*a*). The subharmonic component $\frac{1}{3}\beta$ corresponds to large-scale vortex interaction of the type shown for vortices A″ and A^{iv} (at $t/T = \frac{4}{6}, \frac{5}{6}$). The corresponding time traces of figure 5 ($Re = 900$; $x/L = 0.05, 0.16$) show that the upstream influence at $\frac{1}{3}\beta$ again overshadows that associated with the vortex formation at the instability frequency β.

In summary, the low-frequency component $\frac{1}{3}\beta$, which is the most unstable frequency of stage I oscillation (figure 3; $Re = 250$), exists in stage II (figure 3; $Re = 600$) as well, owing to a remarkable readjustment of the vortex–edge interaction patterns with increasing Reynolds number. This $\frac{1}{3}\beta$ component is associated with large-scale vortex formation at the edge; in stage I they arise from shear-layer instability at $\frac{1}{3}\beta$, while in stage II they stem from selected growth and interaction of the incident vortices of the unstable shear layer at frequency β, giving rise to the vortex patterns described in the foregoing. Over 20 years ago, Powell (1962) showed conceptually the importance of considering the upstream influence from the wedge region in terms of (single) vortex motion there; the observations here appear to corroborate his interpretation. In essence, vortices of circulation Γ at distance L induce upstream perturbations $v_\theta \approx \Gamma/2\pi L$. If we assume that the large-scale vortices described in the foregoing have large Γ, it then follows that the upstream influence of the large-scale $\frac{1}{3}\beta$ vortices will dominate the sensitive region of the shear layer near separation.

This upstream influence of these vortex-interaction patterns on the sensitive region of the shear layer near the nozzle exit (i.e. small x) and consequent growth of unstable disturbances in the shear layer will be addressed in the instantaneous velocity traces and spectral analysis that follow.

Instantaneous velocity traces

Figure 5 illustrates the variation of the transverse fluctuation $\tilde{v}$ with the time t along the jet centreline for $Re = 250$, 600 and 900, corresponding to the flow visualization series of figure 3.

For $Re = 250$, at a location very near the nozzle exit ($x/L = 0.05$), the period of the fluctuation $T_{\frac{1}{3}\beta}$ corresponds to the frequency of formation of vortex pairs at the impingement edge (figure 3*a*) as well as the visualized period of oscillation of the stem of the jet immediately downstream of the nozzle exit. At larger values of x the amplitude of the velocity fluctuation grows (not shown in these normalized traces), and at $x/L = 0.69$ a higher-harmonic component having a period $T_{\frac{2}{3}\beta}$ sets in and persists. Such higher harmonic components are well known to be nonlinear distortions of the fundamental component appearing in non-impinging as well as impinging shear layers (Ziada & Rockwell 1982).

At $Re = 600$ the traces at smaller values of $x/L = 0.05, 0.16$ show dominance of the low-frequency modulation component $\frac{1}{3}\beta$ arising from upstream influence of the large-scale vortex interaction at the wedge (see vortices A, A″, A^{iv} in figure 3*b*). However, the period corresponding to the frequency β of vortex formation in the shear layer is detectable at these small values of x/L, and at $x/L = 0.69, 0.96$ it becomes more pronounced. The well-defined modulation pattern in these latter two velocity traces may be viewed as the superposition of traces corresponding to periods $T_{\frac{1}{3}\beta}$ and T with a prescribed phase shift between them, analogous to the modulation patterns occurring for *single* vortex interactions at a cavity corner (Knisely & Rockwell 1982).

Finally, at $Re = 900$, the patterns of the velocity traces are similar to those of $Re = 600$; again, in this case, there is strong low-frequency modulation at $\frac{1}{3}\beta$ of the

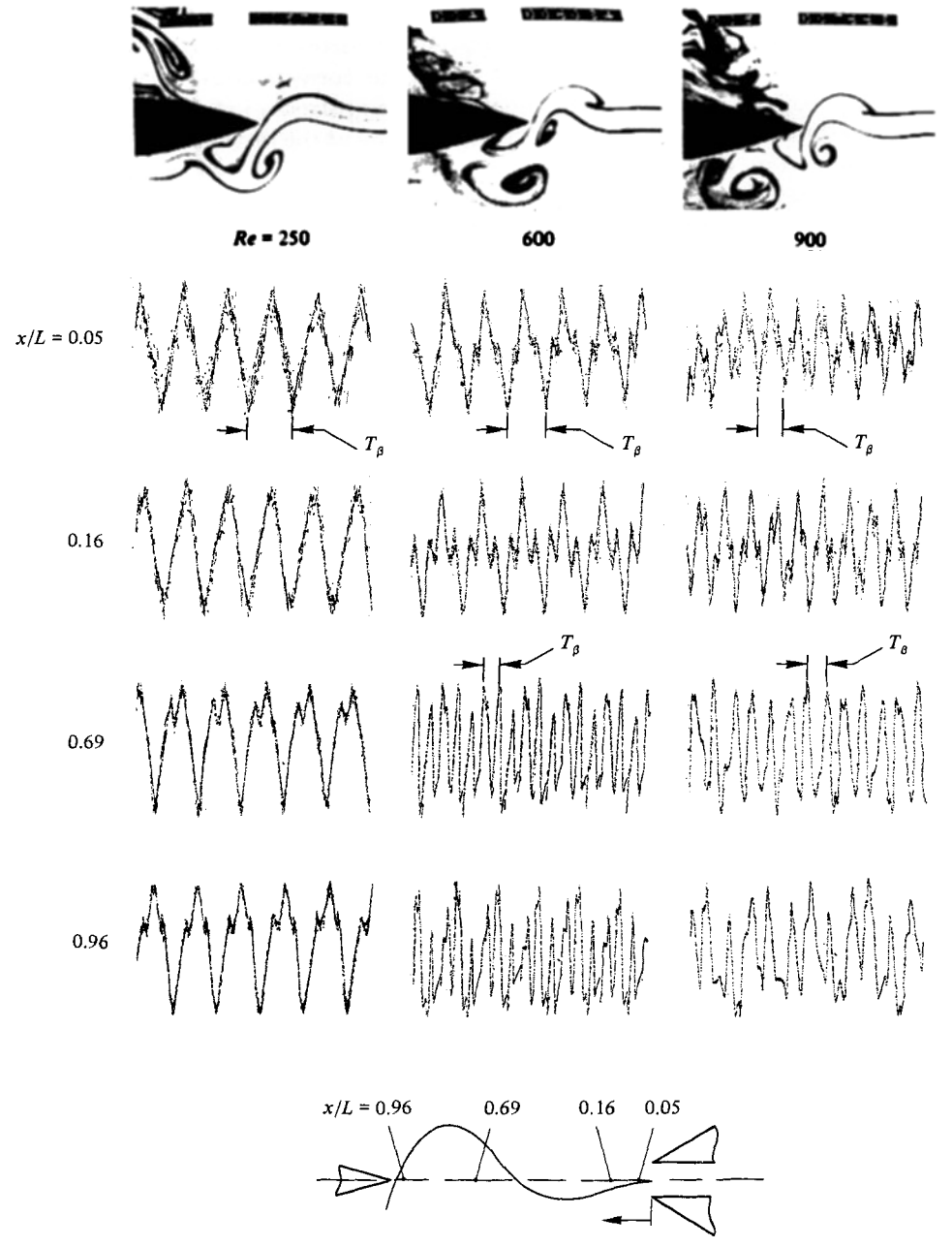

FIGURE 5. Variation of transverse velocity fluctuation $\tilde{v}$ with time t for locations $x/L = 0.05$, 0.16, 0.69, 0.96 along the jet centreline; $Re = 250$, 600 and 900.

separation region of the jet ($x/L = 0.05$, 0.16) due to large-scale vortex interaction at the downstream wedge (see figure 3*c*). At larger values of $x/L = 0.69$, 0.96 (where the scale of the time axis has been expanded relative to the foregoing), the higher-frequency component at T becomes dominant.

On the basis of these velocity traces for stage II oscillations, shown in figure 5 ($Re = 600$ and $Re = 900$), one sees the importance of considering strong modulation

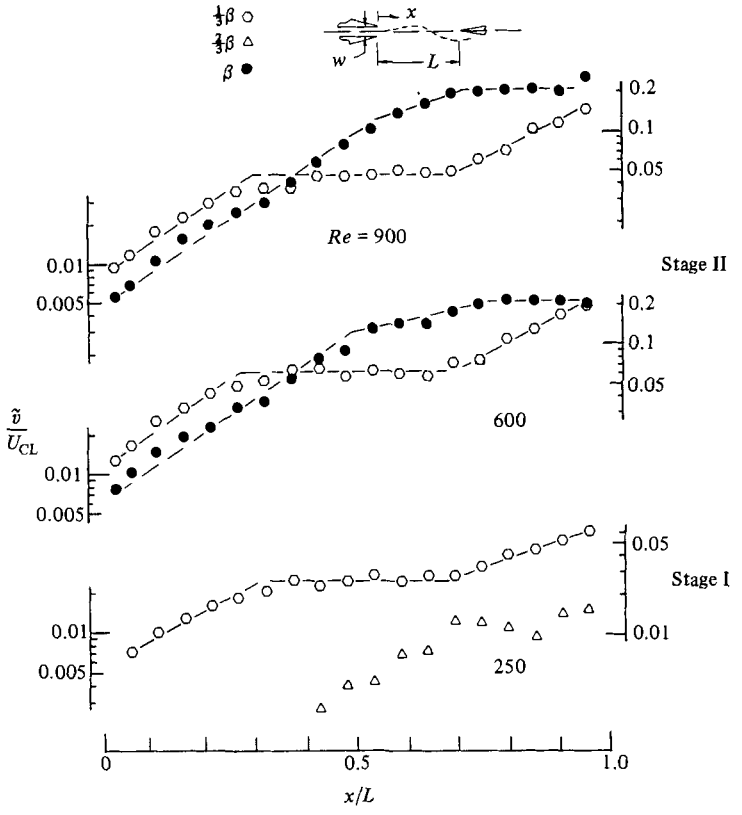

FIGURE 6. Growth rates of velocity amplitudes $\tilde{v}/U$ along jet centreline ($y = 0$) for predominant frequency components of jet oscillation.

at the low frequency $\frac{1}{3}\beta$ of a jet having an unstable frequency β. In §4 we address the growth rates of these predominant components $\frac{1}{3}\beta$ and β, and compare them with linear stability theory.

4. Disturbance growth and modulation

Growth rates of predominant frequency components

Spectral analysis of the velocity fluctuation $\tilde{v}(t)$ typically showed large-amplitude peaks at two or more frequencies. Figure 6 shows the variation of the amplitude of these spectral components as a function of streamwise distance x for $Re = 250$, 600 and 900. At $Re = 250$ there is predominance of component $\frac{1}{3}\beta$ for all values of x, and at sufficiently large x the amplitude of the first harmonic $\frac{2}{3}\beta$ becomes significant. At $Re = 600$ our foregoing considerations revealed that the component $\frac{1}{3}\beta$ becomes a low-frequency modulator of the fundamental instability frequency β; figure 6 shows that the $\frac{1}{3}\beta$ dominates the β-component in the initial growth region of the disturbance, while further downstream the β-component prevails. At $Re = 900$ the streamwise growth of these frequency components is relatively similar to $Re = 600$. These amplitude variations of components $\frac{1}{3}\beta$ and β at each value of Re in figure 6 are similar to the trends indicated by the corresponding time traces in figure 5. Below, the growth rates of these predominant components near the nozzle exit are compared with linear stability theory.

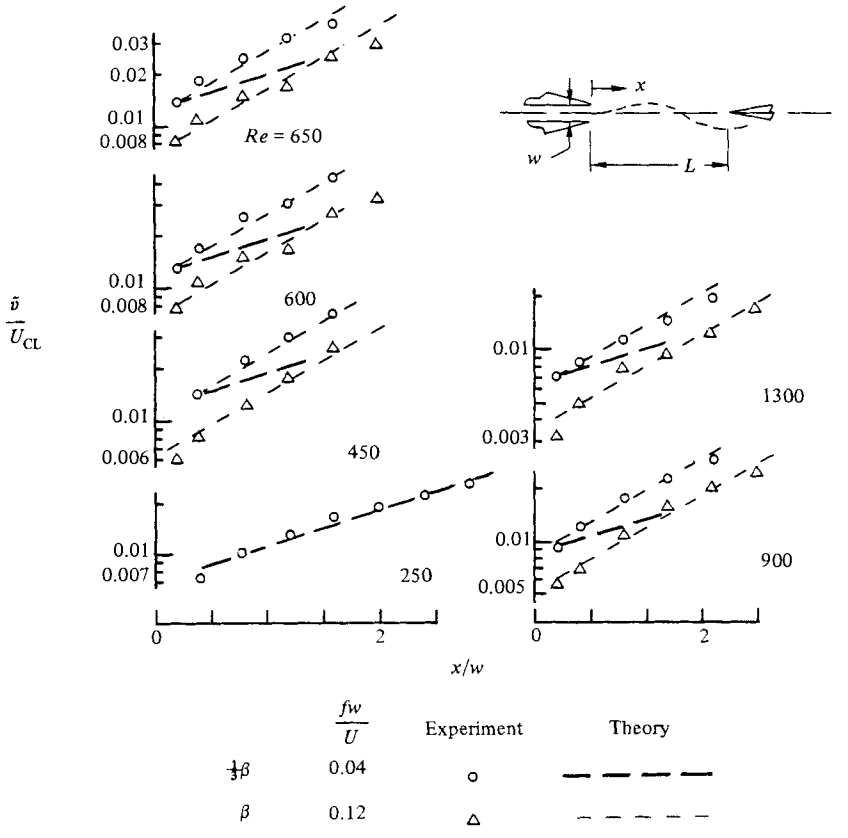

FIGURE 7. Comparison of growth rates of $\tilde{v}/U$ in linear region of disturbance amplification for predominant frequencies of oscillation β and $\frac{1}{3}\beta$ at $Re = 250$, 450, 600, 900 and 1300.

Comparison of disturbance growth rates with linear theory

At small values of x we expect the disturbance growth rates to be described by linear stability theory (Bajaj & Garg 1977). Although both spatial and transformed temporal-amplification factors are shown in figure 2, spatial theory is considered to be more representative for these rapidly amplifying disturbances. Consequently, the theoretical growth rates of figure 7 are based upon the inviscid spatial theory of Bajaj & Garg. At $Re = 250$ the theoretical growth rate at frequency $\frac{1}{3}\beta$ conforms well with the experimental data. (At the location closest to the nozzle exit ($x/L = 0.05$) the low fluctuation level precluded accurate measurement.) However, at higher values of $Re = 450$–1300 the frequency component $\frac{1}{3}\beta$ does not grow at its own rate predicted by linear theory; rather, it follows closely the growth rate of the β-component. This reaffirms our view that the low-frequency component $\frac{1}{3}\beta$ simply modulates the oscillation of the most unstable frequency β instead of growing independently.

Here we see an analogy with the experimental observations of Knisely & Rockwell (1982) for flow past a cavity. In their study a similar type of low-frequency modulation occurred; however, the amplitude of the modulating component was always substantially less than that of the most unstable frequency of the shear layer. The upstream modulation at low frequency was simply due to small perturbations in single-vortex–cavity-corner interaction. In the present investigation, the strong upstream influence arises from the interaction between a number of vortices at the edge, as shown in the foregoing.

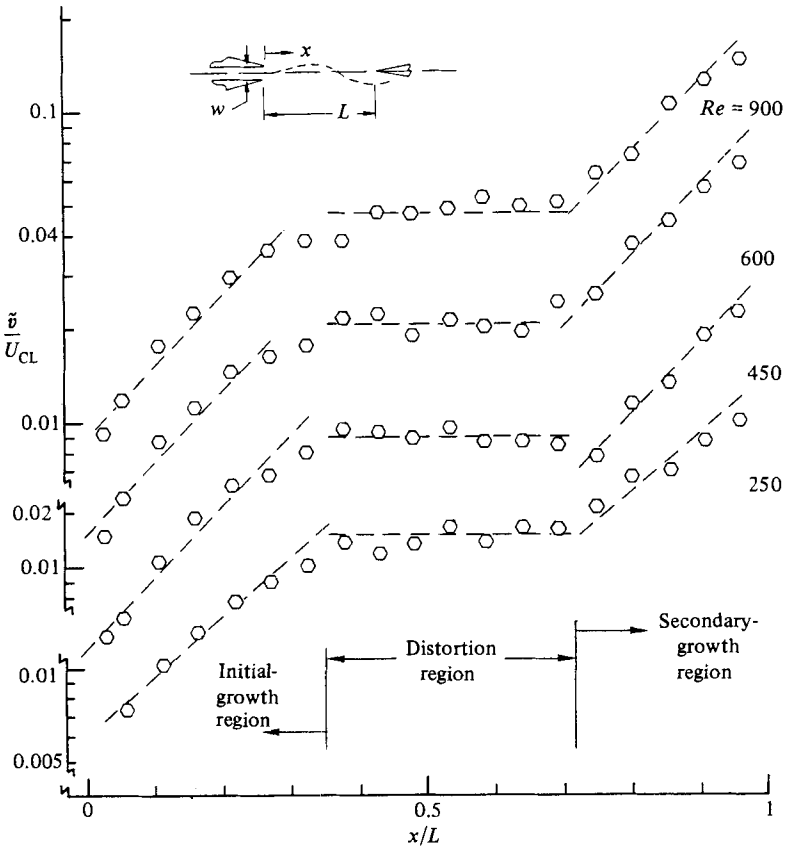

FIGURE 8. Growth of low-frequency modulating component $\frac{1}{3}\beta$ of normalized velocity $\tilde{v}$ along centreline ($y = 0$) for Re = 250, 450, 600 and 900.

Growth of the low-frequency modulating component

Figure 8 shows the amplitude variation of $\tilde{v}(x)$ at the low-frequency component $\frac{1}{3}\beta$. Remarkable is the persistence in shape of the amplitude distributions over a nearly fourfold range of Re. In all cases there is a secondary-growth region immediately upstream of the jet edge; the corresponding growth rates are nearly parallel for the three highest values of Re. In fact, these growth rates are well predicted by linear stability theory for the $\frac{1}{3}\beta$-component! Critically speaking, however, this agreement must be regarded as fortuitous, since we expect the disturbance growth to be governed by nonlinear phenomena in this region.

The unusual nature of this secondary-growth region, taken together with the relatively constant disturbance amplitude in the 'distortion region' (figure 8) calls for examination of the distributions of $\tilde{v}(y)$ across the shear layer to determine the degree to which they depart from their initial shapes in the linear-growth region. Figure 9(*a*) shows variation of $\tilde{v}(y)$ for the two primary components $\frac{1}{3}\beta$ and β. In the region close to the nozzle exit, represented by $x/L \lesssim 0.3$, the eigenfunction distributions $\tilde{v}(y)$ have a qualitatively similar shape, with the maximum occurring at the jet centreline. This trend approximates well that of linear theory (Mattingly & Criminale 1971). Although distributions of $\tilde{v}(t)$ calculated from linear theory are not available in Bajaj & Garg's (1977) spatial study, the eigenfunction distribution of Mattingly & Criminale, albeit for a lower-Reynolds-number jet, does show a

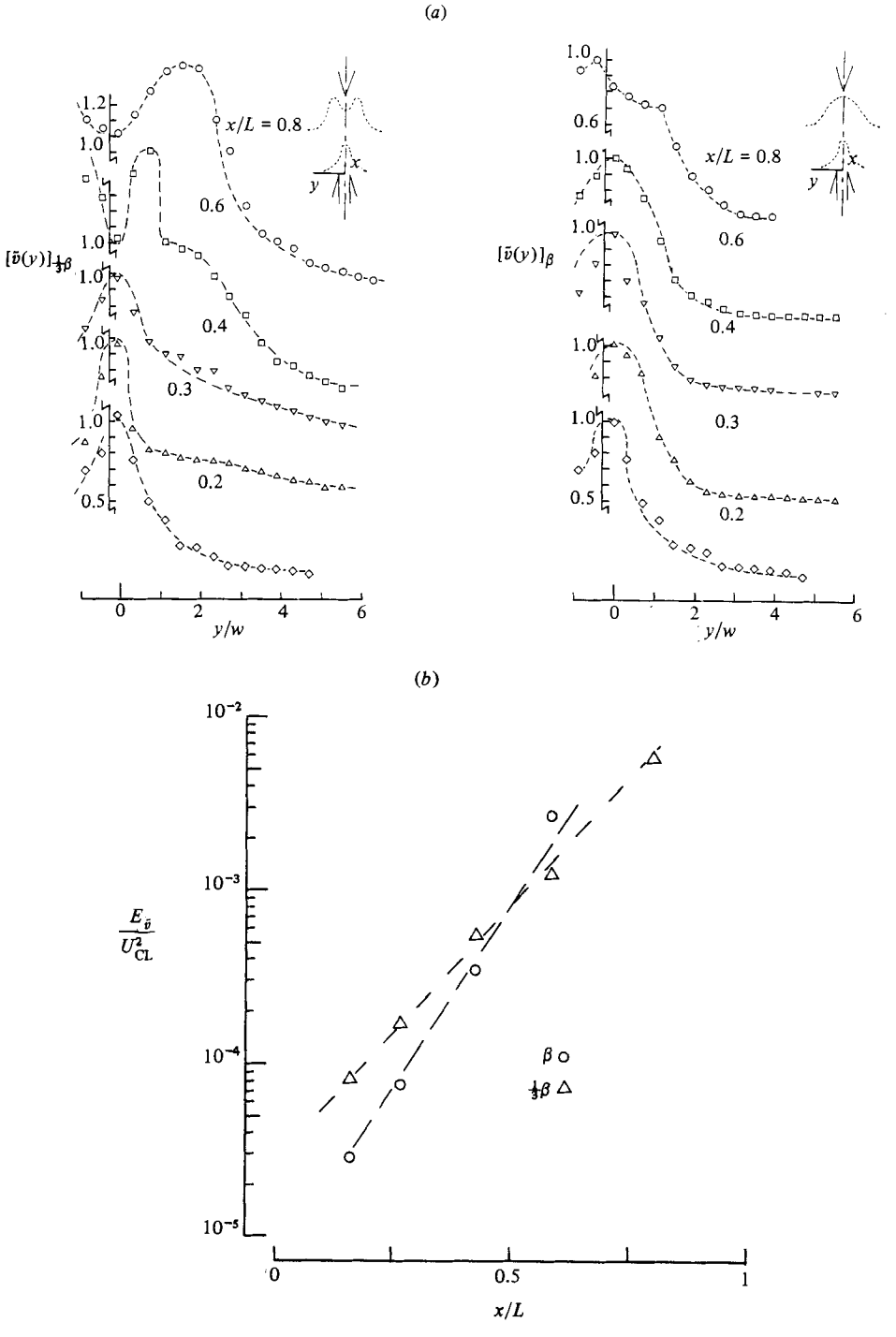

FIGURE 9. (*a*) Distribution of velocity fluctuation $\tilde{v}(y)/U$ across the jet for low-frequency modulating component $\frac{1}{3}\beta$ and most-amplified component β at $x/L = 0.2$, 0.3, 0.4, 0.6, 0.8 for $Re = 650$. (*b*) Integrated kinetic energy $E_{\tilde{v}}$ of distributions of (*a*).

generally similar variation to the data of figure 9(*a*) at small x/L. At larger values of x/L it is evident that the general shape of the $\tilde{v}(y)$ distribution at the most unstable frequency β is preserved. On the other hand, there are marked alterations in the shape of $\tilde{v}(y)$ for the low-frequency modulating component $\frac{1}{3}\beta$. Consequently, the 'secondary-growth' region of figure 8 is associated with a $\tilde{v}(y)$ markedly different from that in the classical linear region near the nozzle exit. These observations are associated with the onset of large-scale vortex formation as the edge is approached (see figure 3*b*, $Re = 600$).

Figure 9(*b*) gives the growth rates of the integrated kinetic energy $E_{\tilde{v}} = \int_{-\infty}^{\infty} \tilde{v}^2(y)\,\mathrm{d}y$. Comparing these distributions with those of figure 6, it is evident that the centreline amplitude of $\tilde{v}$ is a reasonably accurate representation of the growth and energy level of the β-component over the entire region from jet separation to impingement. However, for the low-frequency modulating component $\frac{1}{3}\beta$, the centreline amplitude is an accurate indicator only in the initial linear growth region. The severe change in shape of the $\tilde{v}(y)$ profile in the 'distortion region' of figure 8 is actually a region of continuously increasing kinetic energy $E_{\tilde{v}}$.

5. Nonlinear interactions and multiple frequencies

Up to this point, we focused on the primary frequency components $\frac{1}{3}\beta$ and β within the oscillating jet. However, detailed frequency spectra taken throughout the jet revealed a number of lower-amplitude, but nevertheless well-defined, frequency components, in some cases, as many as seven discrete components were evident, all of them having an amplitude at least 10 % of the maximum primary component. These additional discrete components are central to the energy-transfer process characteristic of transition from laminar to turbulent flow (Miksad 1973; Miksad *et al.* 1982; Knisely & Rockwell 1982).

Figure 10 represents the relative amplitude of each of these frequency components along the jet centreline by the diameter of the data symbol; these diameters were determined from spectra of the type shown at the bottom of figure 10. At a given value of x/L the component with the largest amplitude has the largest-diameter symbol. Smaller-diameter symbols of the remaining components at that value of x/L represent proportionally smaller amplitudes of the respective frequency components. Only those frequency components having an amplitude at least 10 % that of the maximum-amplitude (primary) component are included in these plots.

The left-hand ordinate of each plot gives the absolute value of Strouhal number fw/U of each frequency component, and the right-hand ordinate shows the particular frequency component in terms of the primary frequency β. All components, for all values of Re, can be represented as sums of β and $\frac{1}{3}\beta$. Possible relations are

$$\left.\begin{aligned} &\tfrac{1}{3}\beta, && \tfrac{5}{3}\beta = \beta+\tfrac{2}{3}\beta,\\ &\tfrac{2}{3}\beta = \tfrac{1}{3}\beta+\tfrac{1}{3}\beta, && \tfrac{6}{3}\beta = \beta+\beta,\\ &\tfrac{3}{3}\beta = \beta, && \tfrac{7}{3}\beta = 2\beta+\tfrac{1}{3}\beta\\ &\tfrac{4}{3}\beta = \beta+\tfrac{1}{3}\beta, \end{aligned}\right\} \qquad (1)$$

The first harmonic of β, i.e. 2β, may be viewed as evolving from nonlinear distortion of the fundamental β. Biocoherence analysis shows that it may also be interpreted as an interaction with itself; i.e. $2\beta = \beta+\beta$ (Knisely & Rockwell 1982). Of course, certain components of (1) can also be represented as difference combinations of β and

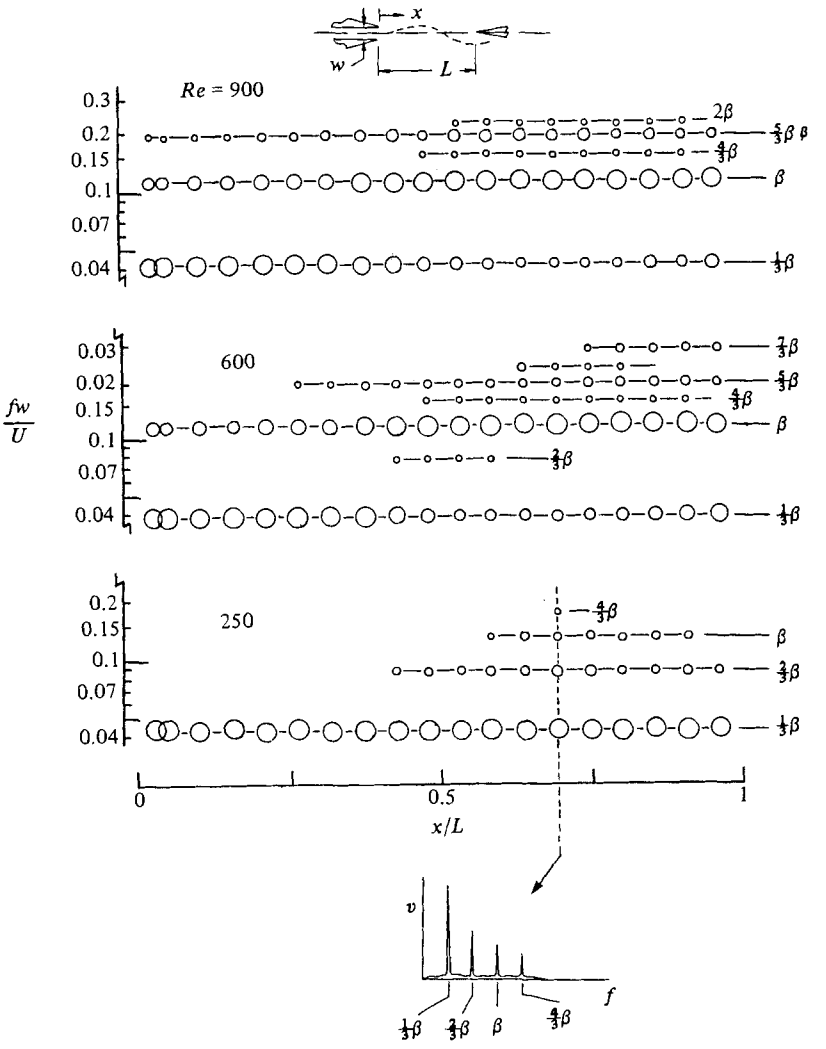

FIGURE 10. Multiple-frequency components arising from nonlinearity of component $\frac{1}{3}\beta$ ($Re = 250$) and nonlinear interaction of primary components β and $\frac{1}{3}\beta$ ($Re = 600$ and 900).

$\frac{1}{3}\beta$, e.g. $\frac{4}{3}\beta = 2\beta - \frac{2}{3}\beta$. Irrespective of the type of interpretation, all sum and difference possibilities show that nonlinear wave interaction between β, $\frac{1}{3}\beta$ and their combinations is an admissible source of the components given in figure 10 and (1). In the following, we discuss further details of these components, commencing with the lowest Reynolds number.

At the lowest Reynolds number $Re = 250$, the primary component $\frac{1}{3}\beta$ and its first, second and third harmonics $\frac{2}{3}\beta$, β and $\frac{4}{3}\beta$ are present with successively decreasing amplitudes. In other words, these higher-order components are due to distortion of the fundamental $\frac{1}{3}\beta$ at sufficiently high amplitudes of oscillation wherein the $\frac{1}{3}\beta$, $\frac{2}{3}\beta$, $\frac{3}{3}\beta$ and $\frac{4}{3}\beta$ components have successively smaller amplitudes. This type of higher harmonic production is well predicted by Stuart's (1967) inviscid nonlinear theory (also see Ziada & Rockwell 1982). Only if the $\frac{2}{3}\beta$-component were to have an amplitude of the same order as the primary $\frac{1}{3}\beta$-component could we consider it to be a primary component as well; in this case, the $\frac{2}{3}\beta$-component could be viewed as the difference frequency of β and $\frac{1}{3}\beta$.

In fact, at higher Re ($Re = 600$, 900) the aforementioned upstream modulation of the shear layer does indeed give two primary components: $\frac{1}{3}\beta$, the modulating frequency arising from downstream vortex interactions; and β, the most unstable frequency of the jet. At $Re = 600$ there are five components in addition to the primary components $\frac{1}{3}\beta$ and β, both of which have relatively high amplitudes at very small x/L. If these additional frequency components are the products of nonlinear interaction of $\frac{1}{3}\beta$ and β, then they should be related to the sum and difference frequencies of $\frac{1}{3}\beta$ and β. Equation (1) shows that this is indeed the case. At this point we should emphasize that if there is nonlinear interaction between two spectral components, say f_1 and f_2, then both f_1 and f_2 must appear as spectral peaks. In figure 10 this is not the case at all values of x/L at, for example, the interaction $\beta+\frac{2}{3}\beta = \frac{5}{3}\beta$; the $\frac{2}{3}\beta$ component appears over a limited range of x/L because its amplitude is sufficiently large only in that region, in accord with the foregoing amplitude criterion. Rigorously speaking, one should account for the streamwise evolution of the nonlinearly interacting components by considering the integrated kinetic energy across the flow at each streamwise station; this is important because the shape of the eigenfunction varies, in general, with the frequency under consideration. In this spirit, we determined values of $E_{\tilde{v}}$ for all spectral components at $x/L = 0.84$, just upstream of the impingement edge. At this location, the characteristic fluctuation amplitudes $E^* \equiv E_{\tilde{v}}^{\frac{1}{2}}$, normalized with respect to the maximum at frequency β are

$$\frac{E^*_\beta}{E^*_\beta} = 1, \quad \frac{E^*_{\frac{2}{3}\beta}}{E^*_\beta} = 0.43,$$

$$\frac{E^*_{\frac{1}{3}\beta}}{E^*_\beta} = 0.79, \quad \frac{E^*_{\frac{4}{3}\beta}}{E^*_\beta} = 0.22, \quad \frac{E^*_{\frac{5}{3}\beta}}{E^*_\beta} = 0.21.$$

The basic features of the nonlinear interactions described in conjunction with figure 10 are similar to those observed for shear layers externally excited (via a loudspeaker) at two independent frequencies (Miksad 1973). The important point here is that the two 'excitation frequencies' $\frac{1}{3}\beta$ and β are themselves self-generated in (i.e. inherent to) the flow system, and are present with substantial amplitude, even near shear-layer separation, owing to upstream influence from the flow-edge interaction region. In cases without an edge, one must still admit significant upstream influence from the downstream vortex dynamics (Rockwell 1983); this aspect deserves further investigation. Further details of these interpretations of nonlinear interaction can be found in the related impinging and non-impinging shear-layer studies of Knisely & Rockwell (1982), Miksad (1983) and Miksad *et al.* (1982), addressing cavity and wake flows respectively.

6. Frequency jumps and multiple frequencies

The concept of frequency jumps and hysteresis effects in jet-edge systems was first addressed rigorously by Powell (1971), and has subsequently received considerable attention, as summarized by Rockwell (1983). Although efforts have been largely focused on the variation of a single predominant frequency component in characterizing these jumps and hysteresis effects, we propose here an additional criterion: a sudden increase in the number of multiple frequencies corresponds to a jump to a higher stage of oscillation and *vice versa*. Figure 11 shows the frequencies of those spectral peaks having an amplitude at least 10% of the maximum amplitude component. In accordance with the concepts discussed in conjunction with figure 10,

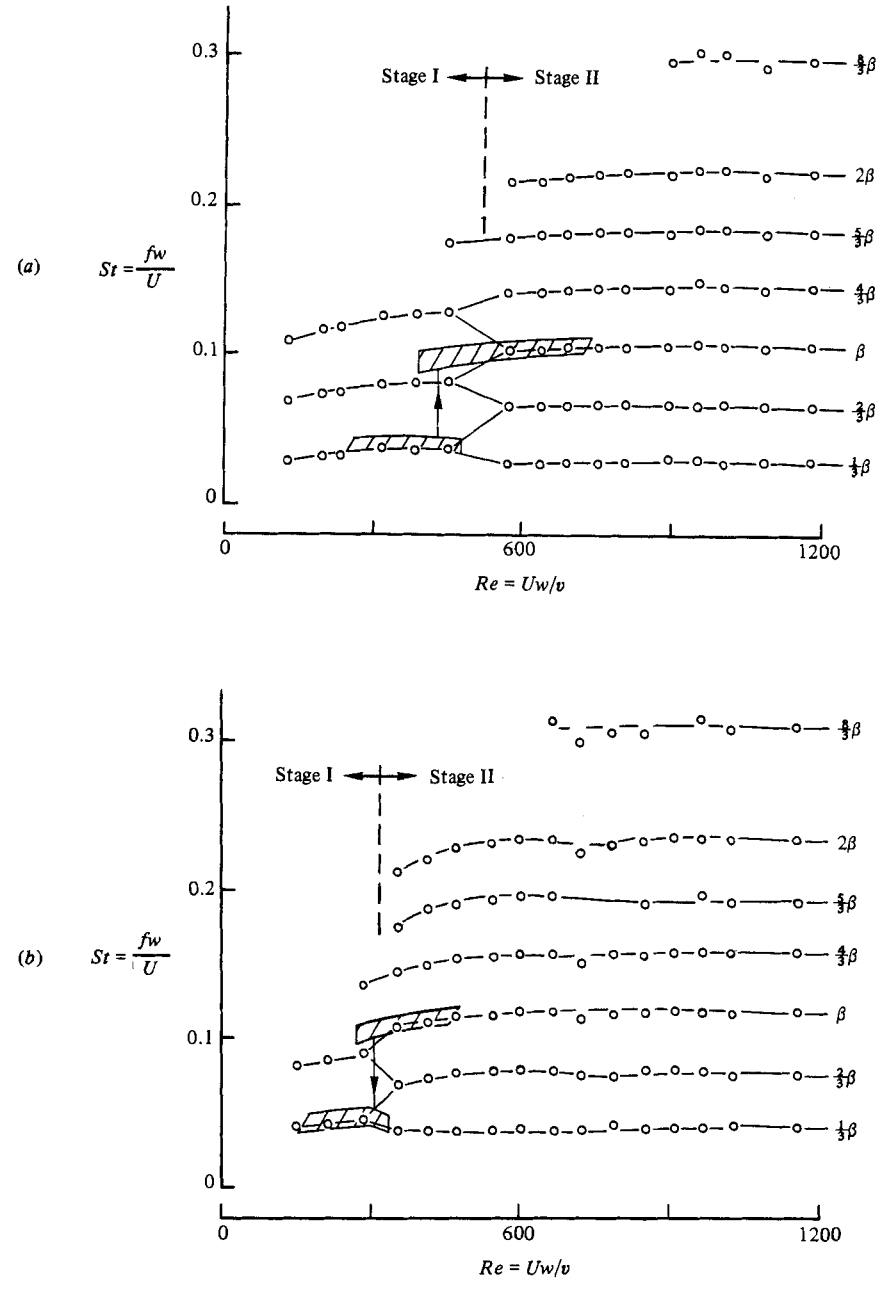

FIGURE 11. Multiple-frequency content of oscillating jet (u-component) at $x/L = 0.75$ on centreline ($y = 0$) illustrating relation between frequency jumps and multiple frequency content as flow passes from (a) stage I to stage II with increasing Re; (b) stage II to stage I with decreasing Re.

there is not a single predominant frequency at this location in the jet. Figure 11 (a) reveals that for increasing Re there is a sudden increase in the number of frequency components in the range $450 < Re < 550$, while figure 11 (b) reveals that for decreasing Re there is a sudden decrease in the number of frequency components in the range $300 \lesssim Re \lesssim 375$. In fact, these two ranges of Reynolds number are very close to the values for which Powell observed upward and downward jumps respectively in

predominant frequency of oscillation on the basis of far-field microphone measurements; they are indicated by the vertical arrows in figure 11. The cross-hatched regions define the range of Powell's data for three different jet breadth-to-width ratios. It is evident from overlap of the boundaries of these regimes that the location of the jump depends on this ratio.

7. Conclusions

The self-excited jet, whose oscillation amplitude is strongly enhanced by its impingement upon a downstream edge, can give rise to a number of well-defined frequency components. Although certain of them may have amplitudes of only 10% of the dominant components of the oscillation, their role is still important; they are associated with the energy transfer between the dominant frequency components as the flow evolves in the streamwise direction. In fact, the absolute amplitudes of the dominant components will be related to the degree of energy transfer between themselves as well as to other components within the jet.

At relatively low values of Reynolds number there is a single predominant frequency of oscillation that coexists with its higher harmonics. These harmonics are simply due to strong nonlinearity of the jet oscillation. Associated with this single predominant component are single, well-defined vortices impinging upon the edge region. Each of these vortices, in turn, produces a large-scale vortex of opposite sense due to the unsteady pressure gradient imposed upon the viscous layer of the edge by impingement of the incident vortex; the result is a 'counter-rotating vortex pair'. Further downstream of the edge, these vortex pairs can, in turn, undergo interaction. The importance of these downstream interactions, or 'secondary instabilities', comes forth at higher values of Reynolds number; they move closer to the impingement edge where they have a drastic effect on the upstream dynamics of the flow.

At higher values of Reynolds number, vortices in the incident jet shear layer develop more quickly, and the corresponding vortex pattern at the edge is considerably more complex. It involves interactions between vortices of the unstable jet shear layer and induced vortices of opposite sense at the edge to produce large-scale low-frequency vortices that have a strong upstream influence. In fact, the sensitive region of the shear layer near the upstream separation edge, where linear amplification of the unstable disturbance occurs, shows two well-defined frequency components: one corresponding to the low-frequency effect of the large vortices at the edge, and the other to the inherent instability of the jet shear layer. As the flow evolves downstream, the interaction between these two strong components gives rise to a number of additional frequency components.

Particularly remarkable is the fact that the vortex-interaction pattern at the edge undergoes a self-adjustment in order to maintain a low-frequency modulating component over a wide range of Reynolds number. This concept deserves careful consideration for other types of flows having finite lengthscales; the linear-growth region immediately downstream of the separation edge may experience strong amplitude modulation from downstream vortex interactions in these cases as well.

The authors are grateful to the Office of Naval Research for primary support of this research program. They also wish to express their appreciation to the National Science Foundation and the Volkswagen Foundation for initial support, and for providing some of the instrumentation used in the experimental work. Dr Charles Knisely provided a penetrating critique of the manuscript.

REFERENCES

BAJAJ, A. K. & GARG, V. K. 1977 Linear stability of jet flows. *Trans. ASME* E: *J. Appl. Mech.* **44**, 378–384.

KNISELY, C. & ROCKWELL, D. 1982 Self-sustained low-frequency components in an impinging shear layer. *J. Fluid Mech.* **116**, 157–186.

MATTINGLY, G. E. & CRIMINALE, W. O. 1971 Disturbance characteristics in a planar jet. *Phys. Fluids* **14**, 2258–2264.

MIKSAD, R. W. 1973 Experiments on nonlinear interactions in the transition of a free shear layer. *J. Fluid Mech.* **59**, 1–21.

MIKSAD, R. W., JONES, F. L., POWERS, E. J., KIM, Y. C. & KHADRA, L. 1982 Experiments on the role of amplitude and phase modulation during transition to turbulence. *J. Fluid Mech.* **123**, 1–29.

POWELL, A. 1961 On the edgetone. *J. Acoust. Soc. Am.* **33**, 395–409.

POWELL, A. 1962 Vortex action in edgetones. *J. Acoust. Soc. Am.* **34**, 163–166.

ROCKWELL, D. 1983 Oscillations of impinging shear layers. *Invited Lecture at 20th Aerospace Sci. Meeting AIAA, January 1980, Orlando, Florida; AIAA Paper* 81–0047; *AIAA J.* **21**, 645–664.

STEGEN, G. R. & KARAMCHETI, K. 1970 Multiple tone operation of the edgetone, *J. Sound Vib.* **12**, 281–284.

STUART, J. T. 1967 On finite amplitude oscillations in laminar mixing layers. *J. Fluid Mech.* **29**, 417–440.

ZIADA, S. & ROCKWELL, D. 1982 Generation of higher harmonics in a self-oscillating mixing layer–wedge system. *AIAA J.* **20**, 196–202.